Standalone Photovoltaic–Battery DC Fast-Charging Station for Off-Grid Electric Vehicles: Design, Simulation and Consistency Verification

Syed Aiman Haidhar Syed Mohamad Hafiz[1], Norhazilina Bahari[2*], Mohamad Haniff Harun[2]

[1]Faculty of Electrical Technology and Engineering, Universiti Teknikal Malaysia Melaka, Hang Tuah Jaya, 76100 Durian Tunggal, Melaka, Malaysia

[2]School of Technical Foundation and Diploma Studies, Universiti Teknikal Malaysia Melaka, Hang Tuah Jaya, 76100 Durian Tunggal, Melaka, Malaysia

DOI: https://doi.org/10.51584/IJRIAS.2026.11100063

Received: 21 October 2026; Accepted: 26 October 2026; Published: 05 November 2026

ABSTRACT

Fast chargers for electric vehicles are hard to supply in rural areas with a weak or absent grid. This paper presents the design and simulation of a standalone photovoltaic (PV) DC fast-charging station with battery storage. The station combines a 60.2 kWp array (5 modules in series, 29 strings), a boost converter with a tuned perturb-and-observe (P&O) maximum power point tracking (MPPT) controller, a 220.8 kWh lithium iron phosphate (LFP) battery energy storage system (BESS) and a two-port 50 kW charger, sized for four vehicles and 200 kWh per day. The model was corrected for scaling errors, its voltage levels were aligned with the selected components, and the converter parameters were justified at the rated array power. With a duty-cycle step of 0.2% every 5 ms the P&O controller settles in 0.28 s and extracts 99.99% of the available power at standard test conditions and at least 99.97% during steps and ramps of irradiance and temperature. All simulated voltages, currents and powers stay within the datasheet ratings, the power balance closes to within 10^{-6}, and the charging time is 1.5 to 1.6 times the minimum that the 25 kW ports allow. Daily simulations with variable irradiance, cell temperature and a four-vehicle charging profile give an overall PV-to-vehicle efficiency of 83 to 86%. The array meets the daily demand on a partly cloudy day with 4.5 peak sun hours but serves only 74% of it on an overcast day with 3.2 peak sun hours. The results are compared with published off-grid charging studies.

Keywords: Standalone photovoltaic system, electric vehicle fast charging, battery energy storage, MPPT, boost converter, MATLAB/Simulink

INTRODUCTION

Transport electrification is moving faster than the grid that is supposed to feed it. Fast chargers draw tens of kilowatts for each vehicle, and many rural and remote sites have either a weak distribution line or none at all. A photovoltaic (PV) array paired with a stationary battery is the obvious way to power a charger there: the array harvests energy during the day, and the battery decouples generation from the moment a vehicle plugs in (Yap et al., 2022; Atawi et al., 2021). Studies for sites with limited grid access, including rural electrification in Malaysia, point to solar energy as a practical resource (Borhanazad et al., 2013).

Putting such a station together is more than connecting three boxes. The array must be sized against the daily energy demand. A DC–DC converter has to hold the array near its maximum power point while the battery and the chargers pull power from a common DC link. And the whole arrangement has to be modelled well enough so that the results can be trusted before any hardware is bought. Several authors have analysed or designed standalone PV-based charging stations, with and without hydrogen or fuel-cell back-up (Grande et al., 2018; Mehrjerdi, 2019; He & Fathabadi, 2020; Ghotge et al., 2021), but the step-by-step link between component sizing and the behaviour of a detailed circuit-level simulation is rarely documented.

ISSN No. 2454-6194 | DOI: 10.51584/IJRIAS |Volume XI Issue X October 2026

This paper describes the design and simulation of a standalone PV-powered DC fast-charging station for off-grid use. The station combines a 60.2 kWp array, a boost converter with perturb-and-observe (P&O) maximum power point tracking (MPPT), a 220.8 kWh LFP battery energy storage system (BESS) and a two-port 50 kW charger. The contributions are as follows. (i) A documented sizing procedure that links the daily energy demand to the battery, the array and the converter, with the converter parameters justified at the rated array power. (ii) A corrected station model in which the scaling of the battery, charger, controller and measurement blocks is audited and the voltage levels are aligned with the selected components. (iii) A P&O controller tuned and tested under steps and ramps of irradiance and cell temperature. (iv) A documented validation procedure of six checks against the component datasheets, a single-diode PV model, a power balance and a time-scale analysis, together with the overall system efficiency. (v) Simulations with variable irradiance, temperature and a realistic four-vehicle charging profile, and a daily energy balance showing how the array size depends on the solar resource. (vi) A comparison with relevant published studies. The remainder of the paper reviews related work, describes the methodology, presents and discusses the results, and gives conclusions and recommendations.

LITERATURE REVIEW

Solar-powered electric vehicle charging

Solar-powered charging stations have been surveyed extensively. Yap et al. (2022) reviewed the development of solar-powered battery electric vehicle charging stations and the open problems in energy management and grid interaction. In grid-connected stations, a battery and PV generation are used mainly to cut operating cost and to shave the demand taken from the grid; Yan et al. (2019) optimised the operation of a charging station with battery storage and PV to reduce cost, and Hussain et al. (2020) sized the battery of a fast-charging station to ride through power outages. These studies show that storage is what makes a PV-supplied fast charger workable, but they assume that the station remains tied to a grid.

Standalone and off-grid charging stations

Several designs remove the grid altogether. Atawi et al. (2021) analysed and designed a standalone charging station supplied by PV energy, and Grande et al. (2018) assessed the energetic, economic and environmental viability of an off-grid PV-battery station in a case study in Spain. Hydrogen has also been added as a long-term store: Mehrjerdi (2019) combined an electrolyser, hydrogen storage and a fuel cell with PV, and He and Fathabadi (2020) used a fuel cell as a supporting source in a standalone plug-in hybrid charging station. Ghotge et al. (2021) examined off-grid solar charging at long-term parking locations. These works establish the concept; what they report is mainly system-level performance, sizing and economics, with less detail on the converter-level behaviour of the charger bus.

Converters, MPPT and battery charging

A boost converter is the usual interface between a PV array and a higher-voltage DC bus. Design procedures for it are well documented (Santos et al., 2006; Ayop & Tan, 2018), as are the DC–DC topologies suited to electric vehicles and fast-charging stations (Chakraborty et al., 2019). The P&O algorithm is the most common MPPT method because of its simplicity, although it oscillates around the maximum power point and its step size must be chosen with care (Esram & Chapman, 2007; Femia et al., 2005). On the load side, lithium-ion batteries are normally charged with a constant-current followed by a constant-voltage stage, and many variants exist for fast charging (Gao et al., 2019). Simulation of the array itself is usually based on the single-diode equivalent circuit (Villalva et al., 2009).

Research gap

Few studies combine sizing, circuit-level simulation and an explicit check of the simulated magnitudes against the datasheets of the chosen components. This matters because circuit models of power converters, batteries and chargers are easy to mis-scale, and plausible-looking waveform shapes can hide numerically impossible values. The present work addresses this gap for a standalone PV–BESS–charger station.

ISSN No. 2454-6194 | DOI: 10.51584/IJRIAS |Volume XI Issue X October 2026

RESEARCH METHODOLOGY

Overview of the procedure

The work followed the flow in Figure 1. After the scope and objectives were fixed, commercial components were chosen and the battery, the PV array and the converter were sized by hand. The station was then built as a time-domain model with the corrected parameters of Table 2, and the P&O controller was tuned and tested under steps and ramps of irradiance and cell temperature. The results were verified with the six checks of Table 3, and if any check failed, the component values and parameters were revised. Three simulations were run: (a) a dynamic run of 3.2 s with a 10 µs step for the converter, the MPPT and the DC link; (b) a real-time charging run of 2.5 h at standard test conditions (STC: irradiance of 1000 W/m² and a cell temperature of 25 °C) with the two 25 kWh vehicle packs of the original test; and (c) daily runs with a 10 s step for clear, partly cloudy and overcast days with a four-vehicle charging profile. Finally, the results were analysed, the efficiency was calculated and the findings were compared with published studies.

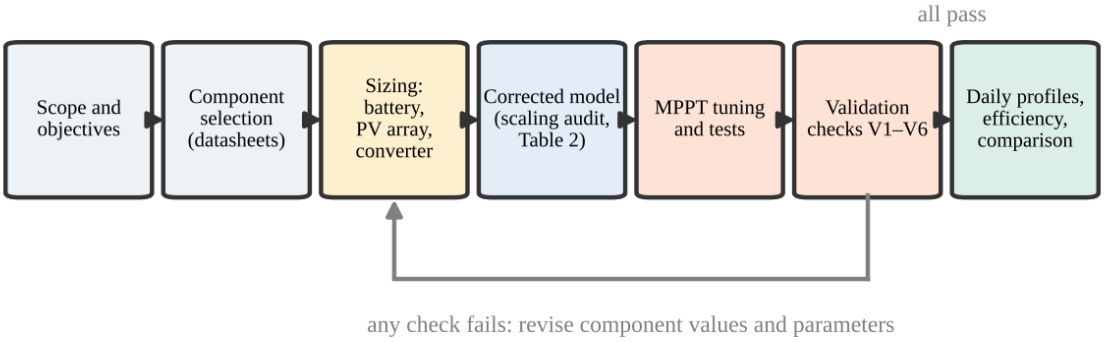


Figure 1: Methodology followed in this study, from the scope definition to the validation checks, efficiency calculation and comparison.

The architecture of the station is shown in Figure 2. The PV array feeds a boost converter through an input capacitor. The perturb-and-observe MPPT block reads the array voltage and current and returns the converter duty cycle. The converter output forms a DC link that is held by the BESS, so the DC-link voltage follows the battery terminal voltage, from about 396 V at 10% state of charge (SoC) to 441 V at full charge, inside the 320–480 V operating window of the BESS. The BESS and the two charger ports are connected to this link in parallel, and each port charges a battery pack that stands in for a vehicle. The array voltage at the maximum power point (313 to 364 V, depending on the cell temperature) is always below the DC-link voltage, so the boost topology can operate over the whole range.

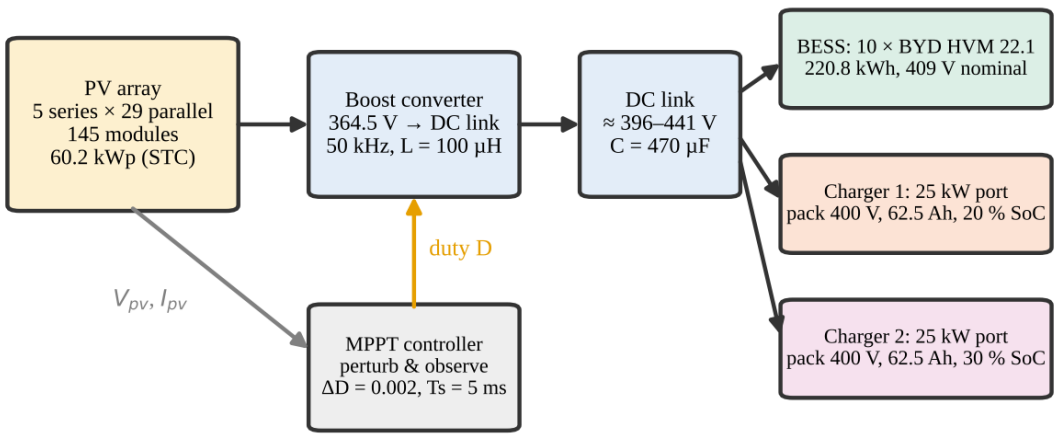


Figure 2: Architecture of the standalone PV–BESS DC fast-charging station.

ISSN No. 2454-6194 | DOI: 10.51584/IJRIAS |Volume XI Issue X October 2026

Components and datasheet values

The components were selected from commercial datasheets (Table 1). The BYD Battery-Box Premium HVM 22.1 uses lithium iron phosphate chemistry. The Siemens VersiCharge Ultra 50 provides 50 kW through two 25 kW ports. The SunPower SPR-415E-WHT-D is a 415 W monocrystalline module. A real vehicle was not modelled; instead, a battery pack of 400 V and 62.5 Ah (25 kWh) represents the vehicle at each port, with start SoC values of 20% and 30% for Charger 1 and Charger 2.

Table 1: Datasheet values of the selected components

Component	Parameter	Value
BESS module (BYD HVM 22.1)	Usable energy; nominal voltage	22.08 kWh; 409 V
	Operating range; maximum output current	320–480 V; 50 A per module
EV charger (VersiCharge Ultra 50)	Output; voltage; efficiency	50 kW (2 × 25 kW); up to 500 V; >92%
PV module (SPR-415E-WHT-D)	P_{max}; V_{mp}; I_{mp}	415 W; 72.9 V; 5.69 A
	V_{oc}; I_{sc}; efficiency	85.3 V; 6.09 A; about 19.2%
	Temperature coefficient of P_{max}	−0.35 %/°C

Battery and PV sizing

The daily energy demand was taken as four vehicles per day at 50 kWh each (Kazem et al., 2013; Shen, 2009):

$$E_{day} = N_{EV} E_{EV} = 4 \times 50 \text{ kWh} = 200 \text{ kWh} \quad (1)$$

Ten BESS modules provide 10 × 22.08 = 220.8 kWh, which covers this demand. At the nominal voltage of 409 V the capacity of one module, following the battery-sizing relation of Kazem et al. (2013) and Leone et al. (2022), is

$$C_{Ah} = \frac{E_{usable}}{V_{nom}} \times 1000 \quad (2)$$

giving 53.98 Ah per module and 539.8 Ah for the ten. The PV array was arranged as five modules in series, so that the string voltage at the maximum power point is 5 × 72.9 = 364.5 V, which is below the DC-link voltage (396 to 441 V) as a boost converter requires, and 29 strings in parallel.

The open-circuit voltage of the array is 426.5 V at STC and about 439 V at a cell temperature of 15 °C, which stays below the 480 V upper limit of the BESS window. The array power at STC, from the series–parallel array relation used for standalone sizing by Shen (2009) and Leone et al. (2022), is which gives 5 × 29 × 72.9 × 5.69 ≈ 60.2 kW from 145 modules covering about 299 m².

$$P_{array} = N_s N_p V_{mp} I_{mp} \quad (3)$$

Boost converter design

The converter has to step the array voltage (364.5 V at the maximum power point) up to the DC-link voltage at a switching frequency of 50 kHz. The design point is the rated array power of 60.2 kW at the upper end of the BESS voltage range (432 V, about 97% SoC), which gives the largest duty cycle at the rated current. The duty cycle, inductance and output capacitance follow from the standard continuous-conduction relations

ISSN No. 2454-6194 | DOI: 10.51584/IJRIAS |Volume XI Issue X October 2026

(Ayop & Tan, 2018; Pradhan & Panda, 2018; Hashim et al., 2018; Chandra Mouli et al., 2017):

$$D = 1 - \frac{V_{in}}{V_o} \tag{4}$$

$$L = \frac{V_{in} D}{f_{sw} \Delta I_L} \tag{5}$$

$$C = \frac{I_o D}{f_{sw} \Delta V_o} \tag{6}$$

where V_{in} and V_o are the input and output voltages, f_{sw} the switching frequency, ΔI_L the inductor current ripple, I_o the output current and ΔV_o the output voltage ripple (taken as 1% of 432 V, or 4.3 V). At the design point D = 0.156, the input current is 165 A and the output current is 139 A; over the cell-temperature and SoC range met in the daily runs the duty cycle varies between 0.12 and 0.29. The inductor was selected for a ripple not above 10% of the rated input current (16.5 A), which requires at least 69 µH. An inductance of 100 µH was adopted, which gives a ripple of 11.4 A (6.9%) at the design point and 9.0 A at a DC-link voltage of 416 V, and keeps the inductor in continuous conduction down to about 3.5% of the rated power (an irradiance of about 35 W/m²).

The output capacitance for a 1% ripple is at least 101 µF; 470 µF was adopted, which keeps the output-voltage ripple below 1 V and leaves margin for load steps. An input capacitor of 1 mF holds the array-voltage ripple below 0.1 V. The initial design had used an input current of 5 A and an output current of 539.8 A (the battery at 1C) in these equations, which do not correspond to the rated operation of the converter, and has therefore been replaced. The resulting values are summarised in Table 4. Equation (4) follows Pradhan and Panda (2018), Equation (5) follows Pradhan and Panda (2018) and Chandra Mouli et al. (2017), and Equation (6) follows Hashim et al. (2018).

Perturb-and-observe MPPT

The P&O algorithm perturbs the converter duty cycle by a small step, observes the change in array power and keeps the direction of the step if the power rose, or reverses it if the power fell. The step ΔD and the sampling period T_s were tuned by simulation (Table 5). ΔD was varied from 0.05% to 1% and T_s from 2.5 to 10 ms, and the settings were compared on the settling time from a start duty cycle of 0.25, the peak-to-peak oscillation of the array voltage and the tracking efficiency under the irradiance and temperature profile of Figure 4. The adopted values are ΔD = 0.2% and T_s = 5 ms. The duty command is compared with a triangular carrier at 50 kHz to generate the gate signal of the converter switch; in the averaged model the duty command is applied directly.

Proposed simulation model

The earlier version of the model returned currents and powers thousands of times above the component ratings and charging that ran two orders of magnitude faster than the 25 kW ports allow. The model was therefore corrected through a scaling audit in which every block was checked for units and gains. All signals are expressed in SI units (V, A, W, s). The battery capacity is entered in ampere-hours and converted to coulombs with a factor of 3600 in the state-of-charge integrator. The charger power command is limited to the port rating and the pack current to 1C, and the measurement blocks have unit gain. The voltage levels are set from the datasheets: the DC link follows the BESS terminal voltage (396–441 V, inside the 320–480 V window), and the pack voltage (340–400 V) stays below the 500 V limit of the chargers. The corrected station is a time-domain model with an averaged boost converter (inductor and capacitor states with conduction, diode and switching losses), the single-diode array of Equation (7), an open-circuit-voltage-plus-resistance model for the BESS and the vehicle packs, and constant-power charger ports with a constant-current stage up to 80% SoC and a tapering constant-voltage stage above it. Table 2 lists the parameters. The array voltage, current and power are obtained from the single-diode model with the cell temperature $T_c = T_a + (NOCT - 20)G/800$, where G is the irradiance, T_a the ambient temperature (25 to 32 °C over the day) and NOCT = 45 °C. Three synthetic days were used: a clear day (6.2 peak sun hours), a partly cloudy day (4.5 peak sun hours) and an

ISSN No. 2454-6194 | DOI: 10.51584/IJRIAS |Volume XI Issue X October 2026

overcast day (3.2 peak sun hours), the last two with passing clouds. Four vehicles arrive at 07:30, 10:30, 14:00 and 18:30, each charging a 62.5 kWh pack from 20% to full (about 50 kWh) on one of the two ports. The PV supplies the chargers first, any surplus charges the BESS and any deficit is drawn from the BESS between 100% and 10% SoC. If the BESS is full the PV is curtailed, and if it is at 10% the chargers are limited to the available PV power. Each day was repeated for eight days from a BESS SoC of 50%, and the last day is reported.

Table 2: Parameters of the simulation model

Block	Parameters	Source
PV array	5 series × 29 parallel SPR-415E modules; single diode, n = 1.0, N_s = 128; R_s = 0.367 Ω, R_{sh} = 512 Ω (per module, at STC); Pmax coefficient −0.35%/°C	Table 1; fitted to datasheet
PV derating	0.95 (soiling, mismatch, DC cables), daily runs only; NOCT = 45 °C	Assumed
Boost converter	L = 100 µH, C_{in} = 1 mF, C_{dc} = 470 µF, f_{sw} = 50 kHz	Table 4
Converter losses	R_L = 8 mΩ, $R_{ds,on}$ = 15 mΩ, V_f = 1.5 V, switching time 200 ns	Assumed (SiC devices)
MPPT	P&O, ΔD = 0.002, T_s = 5 ms, 0.05 ≤ D ≤ 0.5; tracking factor 0.995 in daily runs	Table 5
BESS	539.8 Ah; open-circuit voltage 360 V (0%), 396 V (10%), 409 V (50%), 440 V (100%); R = 12.8 mΩ; coulombic efficiency 0.99; SoC window 10–100%; 500 A limit	Table 1; assumed OCV curve
Chargers	2 × 25 kW from the DC link; efficiency 92%; constant power to 80% SoC, then taper to 12%	Table 1; assumed taper
Vehicle packs	Real-time run: 400 V, 62.5 Ah (25 kWh), 62.5 A limit (1C); daily runs: 62.5 kWh. Pack voltage 340 + 60·SoC V	Table 1; assumed

Verification and validation procedure

The simulated values were judged with the six independent checks of Table 3. First, the scaling of every block was audited (V1). Second, a single-diode model of the array was fitted to the module datasheet and used as the reference for the PV operating point (V4),

$$I = I_{ph} - I_0\left[\exp\left(\frac{V + IR_s}{nN_sV_t}\right) - 1\right] - \frac{V + IR_s}{R_{sh}} \quad (7)$$

where I_{ph} is the photocurrent, I_0 the diode saturation current, R_s and R_{sh} the series and shunt resistances, n the ideality factor, N_s = 128 the number of cells per module and V_t the thermal voltage (Villalva et al., 2009; Toledo et al., 2018; Batzelis, 2019). The parameters were obtained so that the model passes through the datasheet short-circuit, open-circuit and maximum power points, and the array curve was built for five modules in series and 29 strings in parallel. Third, the simulated peak values were compared with the ratings of the corresponding components (V2). Fourth, the speed of the simulated charging was compared with the time that the 25 kW ports would need, through the time-compression ratio (V5), which applies the constant-current charging-energy relation used in EV charging studies (Li et al., 2020; Elma, 2020)

$$\kappa = \frac{t_{rated}}{t_{sim}}, \qquad t_{rated} = \frac{\Delta SoC\, E_{pack}}{\eta\, P_{port}} \quad (8)$$

where ΔSoC is the SoC change of the pack, E_{pack} its energy, η the charger efficiency (0.92) and P_{port} = 25 kW. A physically possible simulation has κ ≤ 1. Finally, the daily energy yield of the array was estimated for a

ISSN No. 2454-6194 | DOI: 10.51584/IJRIAS |Volume XI Issue X October 2026

range of solar resource values from the peak-sun-hour and performance-ratio method (Shiva Kumar & Sudhakar, 2015; Ayompe et al., 2011)

$$E_{pv} = P_{pk}\, H\, PR \tag{9}$$

with P_{pk} the array peak power, H the peak sun hours and PR a performance ratio. The performance ratio was not available from the datasheets and was assumed to lie between 0.70 and 0.80 in this estimate; the simulations give it directly. The power balance (V3) was checked on the dynamic run through the residual, which is the power-balance form used for PV–battery EV charging stations (García-Triviño et al., 2016; Prem et al., 2020)

$$\varepsilon_P = \frac{\int (P_{pv} - P_{loss} - P_{ch} - P_{bat})dt - \Delta E_s}{\int P_{pv}\, dt} \tag{10}$$

where P_{pv} is the array power, P_{loss} the converter loss (conduction, diode and switching), P_{ch} the charger power, P_{bat} the battery terminal power and ΔE_s the change of the energy stored in the capacitors and the inductor. The tracking efficiency of the MPPT was defined, as in Ishaque et al. (2014) and Martinez Lopez et al. (2022), as

$$\eta_{MPPT} = \frac{\int P_{pv}\, dt}{\int P_{mpp}\, dt} \tag{11}$$

where P_{mpp} is the maximum power available at the instantaneous irradiance and cell temperature. The overall efficiency of the station (V6) was defined, following the efficiency accounting of Kymakis et al. (2009) and Dai et al. (2019), as

$$\eta_{sys} = \frac{E_{veh}}{E_{mpp} - E_{curt} - \Delta E_{BESS}} \tag{12}$$

where E_{veh} is the energy delivered to the vehicle packs, E_{mpp} the energy available from the array at its maximum power point, E_{curt} the energy curtailed when the BESS is full and ΔE_{BESS} the change in the energy stored in the BESS. In the daily runs every loss is accounted for separately, and the account must close to within 1%.

Table 3: Validation procedure and acceptance criteria

Check	Description	Acceptance criterion	Equation / table
V1	Scaling and unit audit of every block	Parameters equal the datasheet or Table 2 values; SI units	Table 2
V2	Simulated peak voltages, currents and powers against component ratings	Ratio to the rating ≤ 1.00	Table 6
V3	Power balance of the dynamic run	$\lvert\varepsilon_P\rvert \le 1\%$	Equation (10)
V4	Operating point against the single-diode maximum power point	$P \ge 99\%$ of P_{mpp}; V within 2% of V_{mpp}	Equations (7), (11)
V5	Charging time against the 25 kW port limit	$\kappa \le 1$	Equation (8)
V6	Daily energy account and overall efficiency	Residual ≤ 1%; η_{sys} not above the product of the stage efficiencies	Equation (12); Table 7

RESULTS AND DISCUSSION

Sizing results

Table 4 collects the main design calculations. The sizing logic is self-consistent. The BESS capacity exceeds

ISSN No. 2454-6194 | DOI: 10.51584/IJRIAS |Volume XI Issue X October 2026

the daily demand by about 10%; with the 10% SoC reserve and the 92% charger efficiency holds about 180 kWh for the vehicles, so the station could run for roughly nine tenths of a day without any generation. The array peak power matches the energy demand when about 4.5 peak sun hours are available (see the daily energy balance below).

For the converter, the duty cycle of 0.156 agrees with the initial value. The inductance and capacitance of the initial design were calculated at an input current of only 5 A and an output current of 539.8 A, which do not correspond to the rated operation. At the rated 60.2 kW the input current is 165 A and the output current 139 A, which require at least 69 µH (10% ripple; 23 µH for 30%) and 101 µF. The adopted 100 µH and 470 µF meet these limits with margin, and give an inductor ripple of 11.4 A and an output ripple below 1 V, as justified in the converter design subsection.

Table 4: Design values of the station and recomputed converter components

Item	Initial design	Minimum at 60.2 kW	Adopted
BESS energy	220.8 kWh (10 modules)	—	220.8 kWh
PV array	5 × 29 modules, 60.2 kW	—	5 × 29 modules, 60.2 kW
Duty cycle D	0.16 (0.13–0.20)	0.156	0.156 at 432 V; 0.12–0.29 in operation
Inductance L	777.6 µH (ΔI_L = 1.5 A)	69 µH (10% ripple)	100 µH (ΔI_L = 11.4 A)
Output capacitance	401.7 µF (I_o = 539.8 A)	101 µF (I_o = 139 A)	470 µF
Input capacitance	—	—	1 mF
Switching frequency	50 kHz	—	50 kHz

Minimum values use Equations (4) to (6) with V_{in} = 364.5 V, V_o = 432 V and 1% output-voltage ripple, at the rated array power of 60.2 kW (input current 165 A, output current 139 A). The inductor ripple limit is 10% of the rated input current.

Simulated PV and DC-link behaviour

The array and the DC link were first simulated at STC from a start duty cycle of 0.25. The P&O controller drives the array voltage to 364.2 V within 0.28 s, against a maximum-power-point voltage of 364.4 V from the single-diode model (Figure 3a), and the array delivers 60.14 kW, which is 99.995% of the 60.15 kW available, with a peak-to-peak voltage oscillation of 2.6 V. The operating points at 800 W/m² and 40 °C and at 600 W/m² and 35 °C also fall on the maxima of their curves (Figure 3b). The array voltage and current stay below the open-circuit voltage (426.4 V) and the short-circuit current (176.6 A) of the array; the largest values are 377 V and 172.8 A.

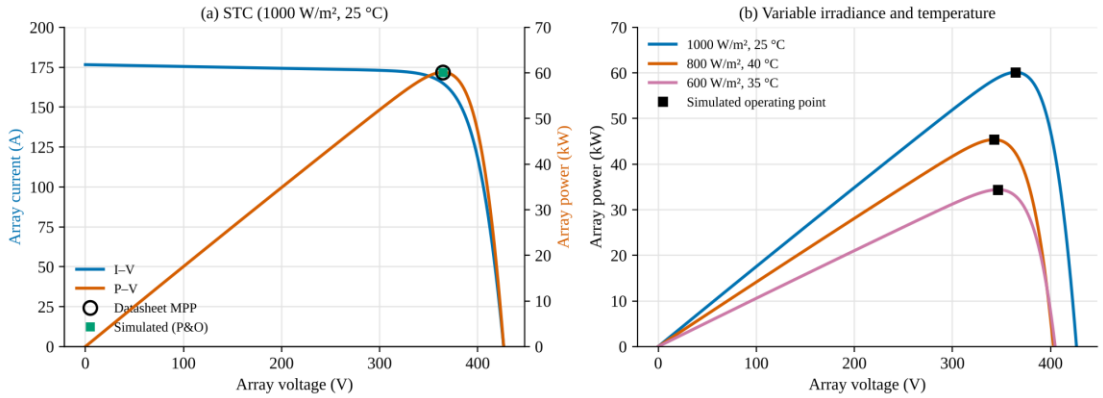


Figure 3: Single-diode I–V and P–V curves of the 5 × 29 array. (a) STC, with the datasheet maximum power point (circle) and the simulated operating point (square). (b) P–V curves for three irradiance and temperature

ISSN No. 2454-6194 | DOI: 10.51584/IJRIAS |Volume XI Issue X October 2026

conditions with the simulated operating points of the P&O controller.

Figure 4 shows the response to steps and ramps of irradiance and cell temperature, with the chargers connected at 0.5 s (50 kW) and one port disconnected at 2.4 s. The array voltage follows the maximum-power-point voltage as it falls from 364 V to about 342 V, with an oscillation of 2.5 to 4.5 V peak to peak that is typical of P&O, and the array power follows the available power (Figures 4a and 4b). The duty cycle moves from 0.13 at STC to 0.18 at 600–800 W/m² (Figure 4c). The DC-link voltage stays between 412.9 V and 415.9 V, the terminal voltage of the BESS at 80% SoC plus the resistive drop, and the BESS current stays between −83 A and +145 A (Figure 4d). The inductor current peaks at 184 A for about 2 ms at start-up, 111% of the rated input current of 165 A, and at 172 A afterwards, so the inductor and the switch should be rated for at least 200 A.

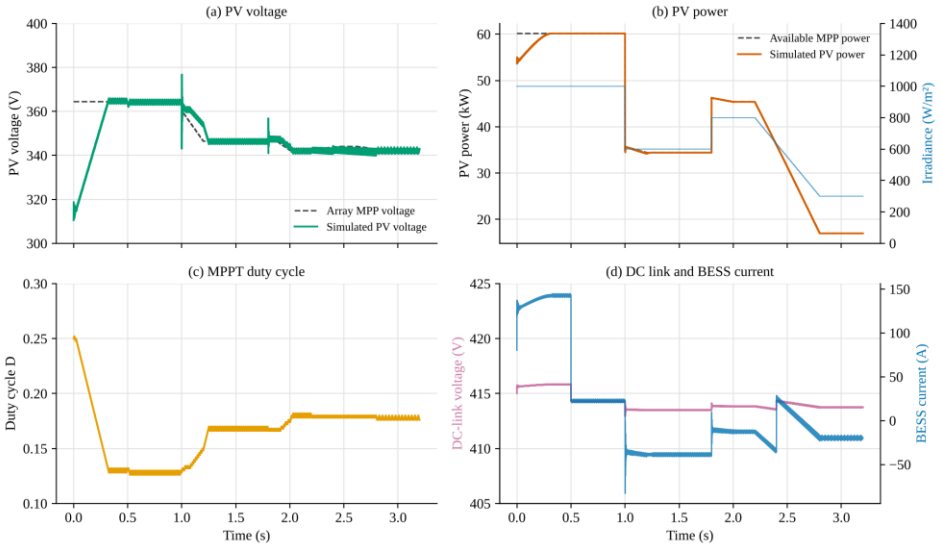


Figure 4: Dynamic response of the station to the irradiance and cell-temperature profile: (a) array voltage, (b) array power with the irradiance profile, (c) duty cycle, (d) DC-link voltage and BESS current.

MPPT tuning

Table 5 shows how the step ΔD affects the tracking at a sampling period of 5 ms. Larger steps converge faster, but the steady-state oscillation grows in proportion and the tracking loss grows with it; with ΔD = 1% the oscillation is 12.8 V peak to peak and the voltage does not stay within 2% of the maximum power point, and with ΔD = 0.05% the controller has not converged after 1 s. A step of 0.2% settles in 0.28 s with an oscillation of 2.6 V and tracks at 99.99% at STC and 99.95% over the steps and ramps. The input network of the converter responds to a duty-cycle step with a rise time of about 0.5 ms, so a sampling period of 5 ms leaves a margin of ten times. A period of 2.5 ms gives almost the same tracking (99.95%, settling in 0.16 s) with less margin, and 10 ms doubles the settling time to 0.59 s and lowers the dynamic tracking efficiency to 99.80%. The initial range of 0.5% to 2% is therefore too coarse for this array. The trade-off between step size and oscillation is the one described for P&O by Esram and Chapman (2007) and Femia et al. (2005).

Table 5: Effect of the P&O step on the tracking (T_s = 5 ms)

ΔD (%)	Settling time (s)	Voltage oscillation (V p-p)	Tracking at STC (%)	Tracking, steps and ramps (%)
0.05	> 1	—	98.41	99.96
0.10	0.56	1.3	99.99	99.77
0.20	**0.28**	**2.6**	**99.99**	**99.95**
0.50	0.13	6.4	99.96	99.96
1.00	not within ±2%	12.8	99.90	99.89

ISSN No. 2454-6194 | DOI: 10.51584/IJRIAS |Volume XI Issue X October 2026

Settling is the time to reach and stay within 2% of the maximum-power-point voltage from D = 0.25. Dynamic tracking is the ratio of the energy extracted to the energy available over 1.0–3.2 s of the profile in Figure 4. The adopted setting is in bold.

Battery and charger behaviour

In the real-time STC run (Figure 5) the BESS starts at 80% SoC and the two 25 kWh packs at 20% and 30%. Both chargers draw their limit from the DC link (25 kW, 23 kW delivered to the pack) until the packs reach 80% SoC, and then taper in the constant-voltage stage; the charger current is limited to 62.5 A (1C) at the start and by the 25 kW port afterwards.

Charger 2 is full after 1.21 h and Charger 1 after 1.33 h. The BESS SoC rises from 80% because the 59.0 kW of PV power exceeds the 50 kW taken by the chargers, and rises faster as the chargers taper, reaching 100% at about 1.5 h.

The SoC curves are monotonic and the charging stops when the packs are full, as expected for a controlled charging process, and the current and power fall as the SoC approaches 100%, in line with the tapering stage of a constant-current constant-voltage profile (Gao et al., 2019).

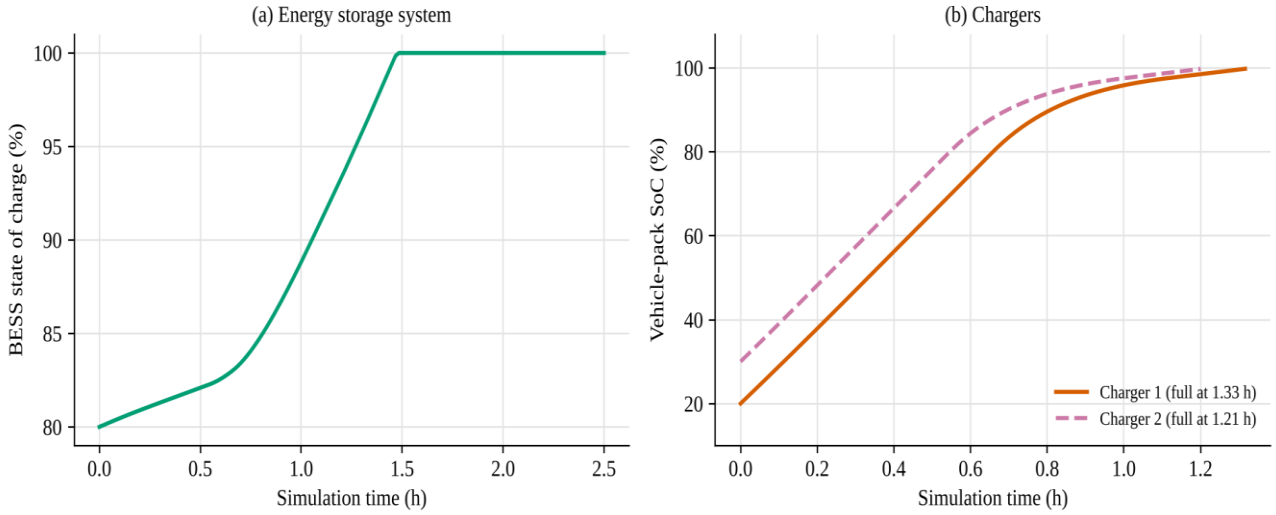


Figure 5: State of charge of (a) the BESS and (b) the two vehicle packs in the real-time run at STC.

Consistency with the datasheet ratings and the power balance

Table 6 compares the peak values of the corrected simulation with the datasheet limits (check V2). All ratios are at or below 1.00. The BESS current peaks at 145 A, against 500 A (ten modules at 50 A), and its power at 60 kW, against about 205 kW. Each charger draws at most 25 kW from the DC link and delivers 23 kW to the pack at 62.5 A and up to 400 V, which is the 25 kW port rating, the 1C current of the pack and 80% of the 500 V limit.

The BESS voltage reaches 441 V at full charge, against 480 V. The power balance (check V3) closes with a residual of 5.4×10^{-7} (0.00005%) over the dynamic run, against the 1% criterion.

At STC (Figure 6a) the 59.0 kW of PV power supplies the 50 kW of the chargers and the remaining 9 kW charges the BESS; as the chargers taper the BESS absorbs up to 59 kW, and once it is full the PV is curtailed. The PV power is therefore above the load whenever the BESS SoC rises, and the power flows close, in contrast with the earlier results.

ISSN No. 2454-6194 | DOI: 10.51584/IJRIAS |Volume XI Issue X October 2026

Table 6: Simulated peak values compared with datasheet or design limits

Quantity	Simulated peak	Reference limit	Ratio
PV voltage	377 V	426.4 V (open circuit at STC)	0.88
PV current	172.8 A	176.6 A (short circuit)	0.98
PV power	60.15 kW	60.15 kW (MPP at STC)	1.00
DC-link voltage	441.3 V	480 V (BESS maximum)	0.92
DC-link power	50.0 kW	50 kW (chargers)	1.00
BESS current	145 A	500 A (10 × 50 A)	0.29
BESS power	60 kW	205 kW	0.29
Charger voltage	400 V	500 V (maximum)	0.80
Charger current	62.5 A	62.5 A (1C of the pack)	1.00
Charger power	25.0 kW per port	25 kW per port	1.00
Time-compression ratio κ	0.66 and 0.63	1 (port limit)	0.66

Ratio is the simulated value divided by the reference limit; all values are at or below 1.00. BESS and charger values are from the real-time STC run and the dynamic run. The PV values are from the dynamic run.

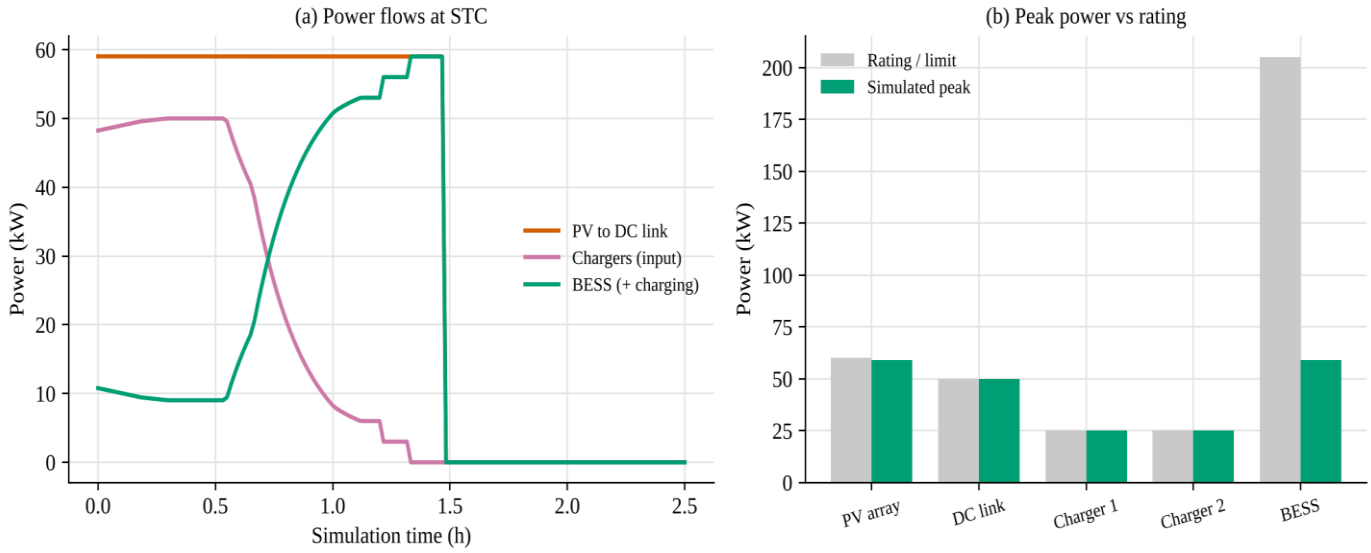


Figure 6: (a) Power flows in the real-time STC run: PV power delivered to the DC link, charger input power and BESS charging power. (b) Simulated peak power of the array, DC link, chargers and BESS compared with their ratings.

Time-scale check

The SoC curves give a second check (V5). A 25 kWh pack going from 20% to 100% takes 20 kWh; at the 25 kW port limit and 92% efficiency (23 kW delivered) this needs at least 3130 s, and Charger 2 (30% to 100%, 17.5 kWh) needs at least 2739 s. In the corrected simulation the charging takes 4779 s and 4373 s, because of the constant-voltage taper above 80% SoC, so the time-compression ratio of Equation (8) is $\kappa = 0.66$ and 0.63, both below 1, whereas the earlier simulation gave about 120 to 160. Figure 7 shows that both curves stay to the right of the lines for the fastest charging that the ports allow.

ISSN No. 2454-6194 | DOI: 10.51584/IJRIAS |Volume XI Issue X October 2026

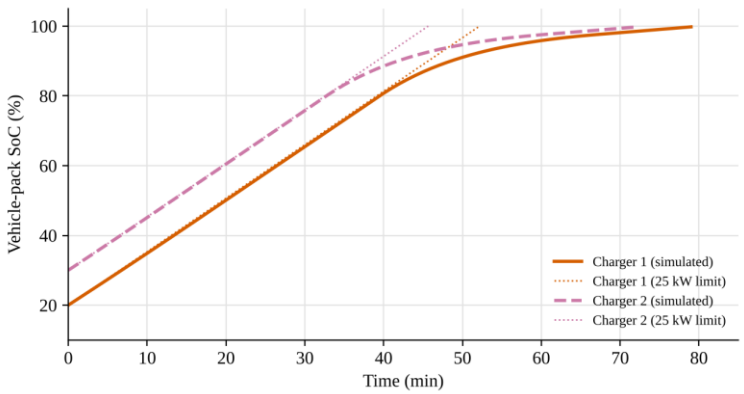


Figure 7: Simulated charging of the two vehicle packs compared with the fastest charging allowed by the 25 kW ports (dotted lines, 92% efficiency).

Operation under variable irradiance, temperature and charging profiles

Figure 8 shows the last of eight repeated days for the clear, partly cloudy and overcast conditions, with the irradiance and cell temperature on the left and the PV, charger and BESS behaviour on the right. The peak PV power on the clear day is only about 49 kW because the cell temperature reaches 63 °C, which lowers the output by about 13% and, with the 5% derating, leaves it well below the 60.2 kWp rating. On the partly cloudy day the PV power changes between near zero and 49 kW within minutes, and the BESS absorbs the changes; its SoC varies between 49% and about 92% and ends the day at 67%, still rising by about 5 kWh per day. On the overcast day the PV supplies only 161 kWh, the BESS sits at its 10% limit, the chargers follow the PV power and only 74% of the demand is served. The DC-link voltage stays between 396 V and 441 V, while the BESS current and power stay below 111 A and 47 kW.

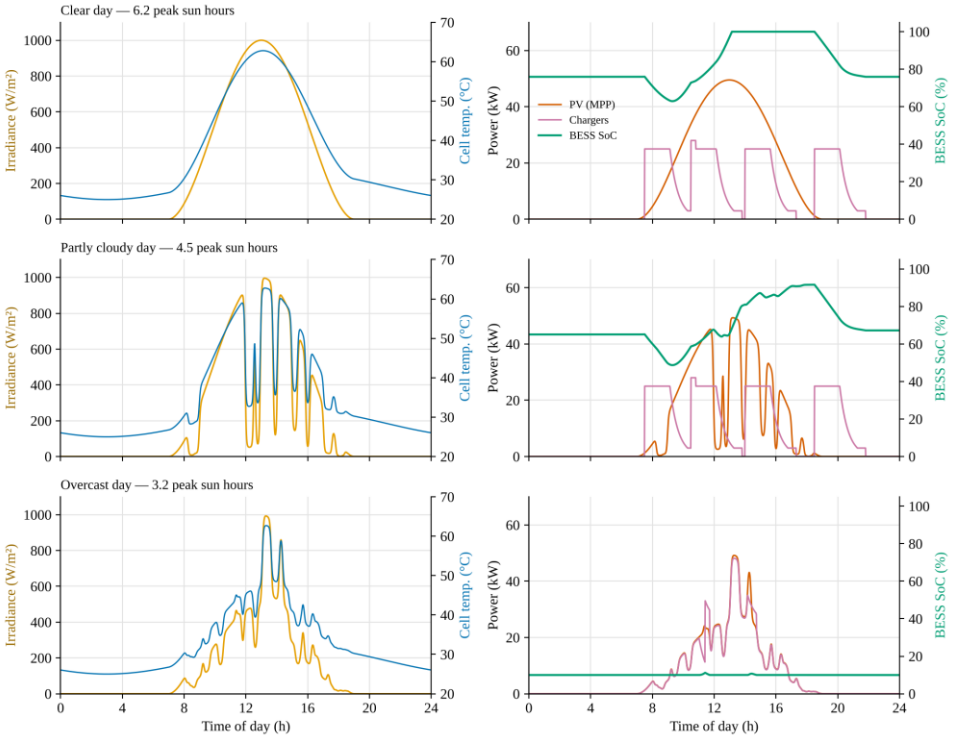


Figure 8: Daily operation for a clear, partly cloudy and overcast day: irradiance and cell temperature (left); PV power at the maximum power point, charger power and BESS SoC (right).

Table 7 gives the energy account of the three days and the overall efficiency of Equation (12) (check V6). The account closes to better than 0.01 kWh. The overall PV-to-vehicle efficiency is 84.6% on the partly cloudy day, 82.6% on the clear day and 85.8% on the overcast day, and it stays below the product of the stage

ISSN No. 2454-6194 | DOI: 10.51584/IJRIAS |Volume XI Issue X October 2026

efficiencies (0.95 derating × 0.995 tracking × 0.986 boost × 0.92 charger = 85.7%, before BESS losses). The charger efficiency of 92% is the largest loss (7.2% of the PV energy on the partly cloudy day), followed by the assumed array derating (5.0%), the boost converter (1.3%) and the BESS (1.1%). The boost converter itself has an efficiency of 98.6% at rated power and 99.0% at 20% of it. On the clear day 27% of the available PV energy is curtailed because the BESS is full.

Table 7: Daily energy account and efficiency of the 60.2 kWp station

Quantity	**Clear**	**Partly cloudy**	**Overcast**
Peak sun hours	6.2	4.5	3.2
PV energy at the maximum power point (kWh)	332.5	240.8	172.6
Array derating, 5% (kWh)	16.6	12.0	8.6
MPPT tracking loss (kWh)	1.6	1.1	0.8
Boost converter loss (kWh)	4.6	3.1	2.0
PV energy curtailed (kWh)	90.5	0.0	0.0
Charger losses (kWh)	17.4	17.4	12.9
BESS losses (kWh)	2.0	2.6	0.1
Change of BESS stored energy (kWh)	0.1	4.8	0.0
Energy delivered to vehicles (kWh)	**199.8**	**199.8**	**148.2**
Demand served (%)	100	100	74
Overall efficiency η_{sys} (%)	**82.6**	**84.6**	**85.8**
Energy-account residual (kWh)	< 0.01	< 0.01	< 0.01
BESS SoC: minimum / end of day (%)	63 / 76	49 / 67	10 / 10
Peak BESS current (A) / power (kW)	111 / 47	110 / 45	111 / 45
DC-link voltage range (V)	411–441	408–423	396–397

Daily energy balance

Table 8 and Figure 9 give the daily balance as a function of the peak sun hours. The simulated runs use the partly cloudy shape scaled to each value and the same four-vehicle profile, and are compared with Equation (9). The simulated performance ratio is 0.83 (PV energy at the DC link divided by $P_{pk}H$), higher than the 0.75 assumed in Equation (9) because the array spends much of the day at a cell temperature well below the midday value. Because the chargers lose 8% of the energy, the vehicles need about 217 kWh at the DC link for the 200 kWh delivered. With the 60.2 kWp array the demand is met in the periodic state at 4.5 peak sun hours or more; at 4.0 and 3.5 hours the station serves 91% and 80% of it. The array needed to serve the full demand throughout a ten-day repetition ranges from 46 kWp at 5.5 hours to 73 kWp at 3.5 hours. The 60.2 kWp design is therefore well matched to a site with about 4.5 peak sun hours and marginal elsewhere. The 220.8 kWh BESS bridges the night and short spells of low irradiance, but it cannot cover a prolonged deficit, as the overcast day shows. The solar resource at the actual site should be taken from measured data before the array is fixed.

ISSN No. 2454-6194 | DOI: 10.51584/IJRIAS |Volume XI Issue X October 2026

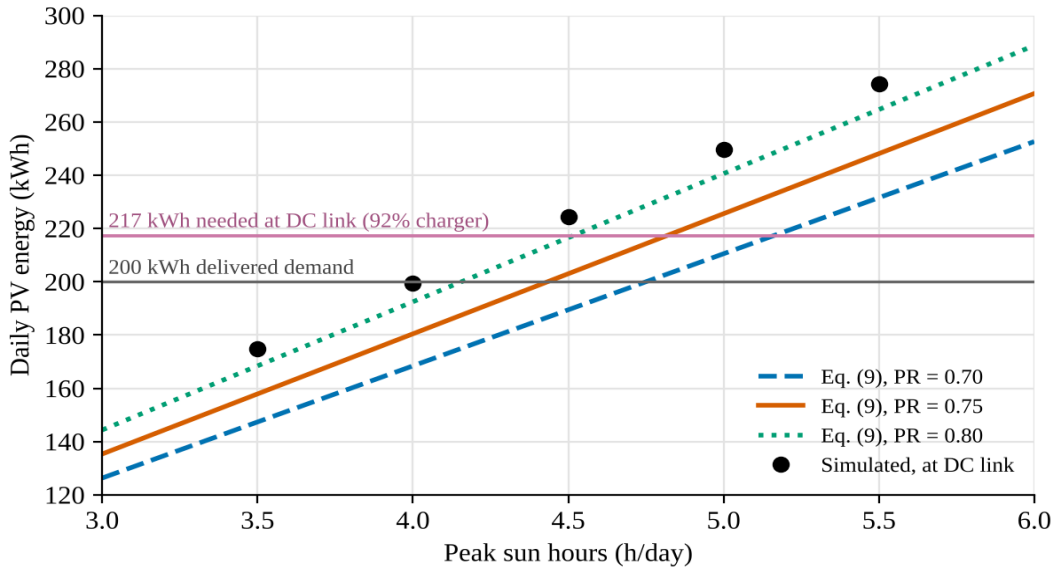


Figure 9: Daily PV energy of the 60.2 kWp array as a function of peak sun hours: Equation (9) for three performance ratios and the simulated energy at the DC link, compared with the 200 kWh delivered demand and the 217 kWh needed at the DC link.

Table 8: Daily energy balance of the 60.2 kWp array as a function of the peak sun hours

Peak sun hours	Equation (9), PR = 0.75 (kWh/day)	Simulated PV energy at DC link (kWh/day)	Delivered to vehicles (kWh/day)	Demand served (%)	Array needed (kWp)
3.5	158	175	160	80	73
4.0	180	200	182	91	64
4.5	**203**	**224**	**200**	**100**	**57**
5.0	226	250	200	100	51
5.5	248	274	200	100	46

Simulated values are for the eighth repeated day; the PV energy at the DC link includes the energy curtailed when the BESS is full. Array needed is the size at which the full demand is served throughout ten repeated days from a BESS SoC of 50%. Equation (9) uses 60.15 kWp.

Comparison with published studies

Table 9 compares the present work with the most relevant standalone studies cited in this paper. Atawi et al. (2021) designed and simulated a 120 W standalone station with a lead-acid battery, boost, buck and bidirectional converters and P&O MPPT, and confirmed the design on a hardware prototype; their transient results are DC-bus settling times of 0.2 to 0.5 s when the PV is connected or disconnected. The present station is about 500 times larger in array power and operates at a 400 V-class DC link; its P&O controller settles in 0.28 s and the DC-link voltage changes by less than 3 V, but it has no hardware verification. Grande et al. (2018) and Mehrjerdi (2019) assess viability and cost at the energy level, with HOMER and with a stochastic optimisation that includes hydrogen and diesel back-up, and do not model the converters; the present work adds the converter and charger level, the datasheet checks and the efficiency. He and Fathabadi (2020) replace the battery with a fuel cell and an electrolyser and use an adaptive-step MPPT; the fixed small step used here converges in 0.28 s, and an adaptive step could shorten this without increasing the oscillation. Ghotge et al. (2021) simulate a full year and find that inadequate charging is rare but more frequent in low-irradiance winter months; the present overcast day, with 74% of the demand served at 3.2 peak sun hours, shows the same

ISSN No. 2454-6194 | DOI: 10.51584/IJRIAS |Volume XI Issue X October 2026

sensitivity to low-irradiance periods, and a year of measured data would be needed to quantify it for this station. We did not find an overall PV-to-vehicle efficiency defined in the same way in these studies, so the 83–86% obtained here (Table 7) is a reference value for 400 V-class standalone stations rather than a figure that can be compared directly. Grid-connected studies (Yan et al., 2019; Hussain et al., 2020) do not address the standalone case.

Table 9: Comparison with published standalone charging-station studies

Study	Scale and configuration	Method	Main finding and comparison with this work
Atawi et al. (2021)	120 W PV, 65 Ah lead-acid battery, boost, buck and bidirectional converters; P&O	Simulink simulation and hardware prototype	DC-bus settling 0.2–0.5 s. This work: 60.2 kWp, 220.8 kWh LFP, 400 V class; settling 0.28 s; no hardware
Grande et al. (2018)	Off-grid PV–BESS for EV charging, Madrid data	HOMER; energetic, economic and environmental analysis	Technically and economically viable. This work adds converter-level behaviour and datasheet checks
Mehrjerdi (2019)	PV with electrolyser, hydrogen storage, fuel cell and diesel back-up	Stochastic cost optimisation	Cost-focused; no converter model. This work gives the electrical behaviour and efficiency
He and Fathabadi (2020)	PV with fuel cell, electrolyser and hydrogen tanks instead of a battery	Adaptive-step MPPT; experiments	Battery replaced by hydrogen. This work uses a BESS and a tuned fixed-step P&O
Ghotge et al. (2021)	Off-grid solar charging at long-term parking	One-year simulation, three allocation strategies	Shortfalls cluster in low-irradiance months. This work: 74% of demand served on an overcast day

Limitations

Several limits apply. The irradiance, temperature and vehicle-arrival profiles are synthetic, so the results show how the station responds rather than how it will perform at a particular site; measured data and a stochastic arrival pattern are needed. The converter is modelled by its averaged equations and fixed loss parameters (Table 2), so switching ripple, thermal behaviour and controller noise are not included, and the converter losses, the 5% array derating and the NOCT are assumptions. The BESS and the vehicle packs use a voltage-source-plus-resistance model without ageing or temperature effects, and the charger efficiency is a constant 92%. The PV analysis relies on a fitted single-diode model with an assumed 128 cells per module and an ideality factor of 1.0, whose fit matches the datasheet to within 0.1% on maximum power and whose temperature coefficient was calibrated to −0.35%/°C. The station has not been verified on hardware.

CONCLUSION AND RECOMMENDATIONS

This study designed and simulated a standalone PV-powered DC fast-charging station with battery storage, corrected the scaling of the model and checked the results against datasheets and first-principles models. The sizing is coherent: a 60.2 kWp array of 145 modules, a 220.8 kWh BESS and a 50 kW two-port charger meet a 200 kWh daily demand when about 4.5 peak sun hours are available. The boost converter was designed at the rated array power (100 μH, 470 μF, 50 kHz), and the P&O controller with $\Delta D = 0.2\%$ and $T_s = 5$ ms converges in 0.28 s and tracks at 99.97% to 99.99% under steps and ramps of irradiance and temperature. All simulated voltages, currents and powers are within the datasheet ratings, the power balance closes to 10^{-6}, and the charging is 1.5 to 1.6 times slower than the fastest that the 25 kW ports allow, as the constant-voltage taper requires. With variable irradiance, cell temperature and a four-vehicle profile, the PV-to-vehicle efficiency is

83 to 86%, limited mainly by the 92% charger efficiency. The array covers the demand on a partly cloudy day with 4.5 peak sun hours, but on an overcast day with 3.2 peak sun hours only 74% is served, and a 60.2 kWp array is marginal below 4.5 hours; about 64 kWp would be needed at 4.0 hours.

Several steps would extend the work. Real irradiance and temperature profiles and a stochastic vehicle arrival pattern should replace the synthetic ones, and an energy-management strategy that decides when the BESS charges and discharges, and which limits the charger power when the BESS is low, should be built on top of the corrected model. An adaptive-step MPPT and partial-shading conditions should be tested. Hardware-in-the-loop tests, vehicle-to-grid operation and an economic analysis are natural later steps.

Acknowledgement/Funding

The authors thank the Faculty of Electrical Technology and Engineering (FTKE) and School of Technical Foundation and Diploma Studies (STEP), Universiti Teknikal Malaysia Melaka, for the facilities and academic support provided during this work. The study received no external funding.

Conflict of Interest Statement

The authors declare that this research was carried out without any commercial or financial relationship that could be taken as a potential conflict of interest.

REFERENCES

1. Atawi, I. E., Hendawi, E., & Zaid, S. A. (2021). Analysis and design of a standalone electric vehicle charging station supplied by photovoltaic energy. Processes, 9(7), 1246. https://doi.org/10.3390/pr9071246
2. Ayompe, L. M., Duffy, A., McCormack, S. J., & Conlon, M. (2011). Measured performance of a 1.72 kW rooftop grid connected photovoltaic system in Ireland. Energy Conversion and Management, 52(2), 816–825.
3. Ayop, R., & Tan, C. W. (2018). Design of boost converter based on maximum power point resistance for photovoltaic applications. Solar Energy, 160, 322–335. https://doi.org/10.1016/j.solener.2017.12.016
4. Batzelis, E. (2019). Non-iterative methods for the extraction of the single-diode model parameters of photovoltaic modules: A review and comparative assessment. Energies, 12(3), 358.
5. Borhanazad, H., Mekhilef, S., Saidur, R., & Boroumandjazi, G. (2013). Potential application of renewable energy for rural electrification in Malaysia. Renewable Energy, 59, 210–219. https://doi.org/10.1016/j.renene.2013.03.039
6. Chakraborty, S., Vu, H.-N., Hasan, M. M., Tran, D.-D., El Baghdadi, M., & Hegazy, O. (2019). DC-DC converter topologies for electric vehicles, plug-in hybrid electric vehicles and fast charging stations: State of the art and future trends. Energies, 12(8), 1569. https://doi.org/10.3390/en12081569
7. Chandra Mouli, G. R., Schijffelen, J. H., Bauer, P., & Zeman, M. (2017). Design and comparison of a 10-kW interleaved boost converter for PV application using Si and SiC devices. IEEE Journal of Emerging and Selected Topics in Power Electronics, 5(2), 610–623.
8. Dai, Q., Liu, J., & Wei, Q. (2019). Optimal photovoltaic/battery energy storage/electric vehicle charging station design based on multi-agent particle swarm optimization algorithm. Sustainability, 11(7), 1973.
9. Elma, O. (2020). A dynamic charging strategy with hybrid fast charging station for electric vehicles. Energy, 202, 117680.
10. Esram, T., & Chapman, P. L. (2007). Comparison of photovoltaic array maximum power point tracking techniques. IEEE Transactions on Energy Conversion, 22(2), 439–449. https://doi.org/10.1109/TEC.2006.874230
11. Femia, N., Petrone, G., Spagnuolo, G., & Vitelli, M. (2005). Optimization of perturb and observe maximum power point tracking method. IEEE Transactions on Power Electronics, 20(4), 963–973. https://doi.org/10.1109/TPEL.2005.850975
12. Gao, Y., Zhang, X., Cheng, Q., Guo, B., & Yang, J. (2019). Classification and review of the charging

strategies for commercial lithium-ion batteries. IEEE Access, 7, 43511–43524. https://doi.org/10.1109/ACCESS.2019.2906117

13. García-Triviño, P., Torreglosa, J. P., Fernández-Ramírez, L. M., & Jurado, F. (2016). Control and operation of power sources in a medium-voltage direct-current microgrid for an electric vehicle fast charging station with a photovoltaic and a battery energy storage system. Energy, 115, 38–48.
14. Ghotge, R., van Wijk, A., & Lukszo, Z. (2021). Off-grid solar charging of electric vehicles at long-term parking locations. Energy, 227, 120356. https://doi.org/10.1016/j.energy.2021.120356
15. Grande, L. S. A., Yahyaoui, I., & Gómez, S. A. (2018). Energetic, economic and environmental viability of off-grid PV-BESS for charging electric vehicles: Case study of Spain. Sustainable Cities and Society, 37, 519–529. https://doi.org/10.1016/j.scs.2017.12.009
16. Hashim, N., Salam, Z., Johari, D., & Ismail, N. F. N. (2018). DC-DC boost converter design for fast and accurate MPPT algorithms in stand-alone photovoltaic system. International Journal of Power Electronics and Drive Systems, 9(3), 1038–1050.
17. He, F., & Fathabadi, H. (2020). Novel standalone plug-in hybrid electric vehicle charging station fed by solar energy in presence of a fuel cell system used as supporting power source. Renewable Energy, 156, 964–974. https://doi.org/10.1016/j.renene.2020.04.141
18. Hussain, A., Bui, V.-H., & Kim, H.-M. (2020). Optimal sizing of battery energy storage system in a fast EV charging station considering power outages. IEEE Transactions on Transportation Electrification, 6(2), 453–463. https://doi.org/10.1109/TTE.2020.2980744
19. Ishaque, K., Salam, Z., & Lauss, G. (2014). The performance of perturb and observe and incremental conductance maximum power point tracking method under dynamic weather conditions. Applied Energy, 119, 228–236.
20. Kazem, H. A., Khatib, T., & Sopian, K. (2013). Sizing of a standalone photovoltaic/battery system at minimum cost for remote housing electrification in Sohar, Oman. Energy and Buildings, 61, 108–115.
21. Kymakis, E., Kalykakis, S., & Papazoglou, T. M. (2009). Performance analysis of a grid connected photovoltaic park on the island of Crete. Energy Conversion and Management, 50(3), 433–438.
22. Leone, C., Peretti, C., Paris, A., & Longo, M. (2022). Photovoltaic and battery systems sizing optimization for ultra-fast charging station integration. Journal of Energy Storage, 52, 104995.
23. Li, Y., Li, K., Xie, Y., … Fu, C., & Liu, B. (2020). Optimized charging of lithium-ion battery for electric vehicles: Adaptive multistage constant current–constant voltage charging strategy. Renewable Energy, 146, 2688–2699.
24. Martinez Lopez, V. A., Žindžiūtė, U., Ziar, H., Zeman, M., & Isabella, O. (2022). Study on the effect of irradiance variability on the efficiency of the perturb-and-observe maximum power point tracking algorithm. Energies, 15(20), 7562.
25. Mehrjerdi, H. (2019). Off-grid solar powered charging station for electric and hydrogen vehicles including fuel cell and hydrogen storage. International Journal of Hydrogen Energy, 44(23), 11574–11583. https://doi.org/10.1016/j.ijhydene.2019.03.158
26. Pradhan, A., & Panda, B. (2018). A simplified design and modeling of boost converter for photovoltaic system. International Journal of Electrical and Computer Engineering, 8(1), 141–149.
27. Prem, P., Sivaraman, P., Sakthi Suriya Raj, J. S., Jagabar Sathik, M., & Almakhles, D. (2020). Fast charging converter and control algorithm for solar PV battery and electrical grid integrated electric vehicle charging station. Automatika, 61(4), 614–625.
28. Santos, J. L., Antunes, F., Chehab, A., & Cruz, C. (2006). A maximum power point tracker for PV systems using a high performance boost converter. Solar Energy, 80(7), 772–778. https://doi.org/10.1016/j.solener.2005.06.014
29. Shen, W. X. (2009). Optimally sizing of solar array and battery in a standalone photovoltaic system in Malaysia. Renewable Energy, 34(1), 348–352.
30. Shiva Kumar, B., & Sudhakar, K. (2015). Performance evaluation of 10 MW grid connected solar photovoltaic power plant in India. Energy Reports, 1, 184–192.
31. Toledo, F. J., Blanes, J. M., & Galiano, V. (2018). Two-step linear least-squares method for photovoltaic single-diode model parameters extraction. IEEE Transactions on Industrial Electronics, 65(8), 6301–6308.
32. Villalva, M. G., Gazoli, J. R., & Filho, E. R. (2009). Comprehensive approach to modeling and simulation of photovoltaic arrays. IEEE Transactions on Power Electronics, 24(5), 1198–1208.

https://doi.org/10.1109/TPEL.2009.2013862

33. Yan, Q., Zhang, B., & Kezunovic, M. (2019). Optimized operational cost reduction for an EV charging station integrated with battery energy storage and PV generation. IEEE Transactions on Smart Grid, 10(2), 2096–2106. https://doi.org/10.1109/TSG.2017.2788440
34. Yap, K. Y., Chin, H. H., & Klemeš, J. J. (2022). Solar energy-powered battery electric vehicle charging stations: Current development and future prospect review. Renewable and Sustainable Energy Reviews, 169, 112862. https://doi.org/10.1016/j.rser.2022.112862